Chapter 5
Sedimentation equilibrium in the analytical ultracentrifuge

Donald J. Winzor

Centre for Protein Structure, Function and Engineering, Department of Biochemistry, University of Queensland, Brisbane, Queensland 4072, Australia.

Stephen E. Harding

NCMH Physical Biochemistry Laboratory, University of Nottingham, School of Biosciences, Sutton Bonington, Leicestershire LE12 5RD, UK.

1 Introduction

For many years analytical ultracentrifugation was the major source of information on the heterogeneity and molecular size of macromolecules. In the field of protein chemistry the question of solute heterogeneity is now usually addressed by gel electrophoretic and gel chromatographic techniques, and the molecular weight is either calculated from the amino acid sequence or obtained by mass spectrometry. Because such molecular weight values refer only to the covalently-linked polypeptide chain(s), they provide no information about the macro-molecular state of the functional protein or enzyme. In its simplest application molecular weight measurement by analytical ultracentrifugation is therefore used to characterize quaternary structure, which affords an example of a self-association equilibrium that has gone to completion.

For many proteins, however, the monomeric and polymeric forms coexist in association equilibrium, the relative proportions of the two macromolecular states varying with total solute concentration in accordance with *Le Chatelier's* principle: the polymeric state is favoured by an increase in concentration, whereas dilution favours the monomeric state. Analytical ultracentrifugation has great potential for characterizing the self-association equilibrium by virtue of these concentration-dependent changes in the average macromolecular state of the solute. The requirement that a rapidly re-equilibrating solute system be characterized without perturbing the equilibrium state is readily accommodated by either of the two commonly used techniques in analytical ultracentrifugation —sedimentation velocity and sedimentation equilibrium. In the former the ultracentrifuge is operated at a sufficiently high angular velocity for the

centrifugal force on a solute molecule to dominate its migration. In sedimentation equilibrium the instrument is operated at a much lower angular velocity to allow a balance to be achieved between the radially-outward flow of solute and the back-diffusional flow in response to the concentration gradient being developed by the centrifugal force.

Despite the greater biological prevalence of interactions between dissimilar macromolecular reactants, protein self-association has been the predominant phenomenon studied by analytical ultracentrifugation. However, the introduction of a new generation of analytical ultracentrifuges has also kindled interest in use of the technique for characterizing interactions between dissimilar reactants. The main emphasis in current ultracentrifuge studies is thus the study of non-covalent macromolecular association equilibria: protein–protein interactions such as those involved in enzyme self-association or the binding of an antibody to its eliciting protein antigen; protein–nucleic acid interactions such as those associated with regulation of the transcription and translation of genetic information; and protein–carbohydrate interactions such as those between a lectin and the sugar moiety of a glycoprotein.

2 Experimental aspects of sedimentation equilibrium

As noted above, the sedimentation equilibrium variant of analytical ultracentrifugation entails operation of the instrument at a relatively low angular velocity that allows the centrifugally driven flow of solute to be matched by the diffusion-driven counterflow in response to the gradient in solute concentration being generated by the sedimentation process. From the viewpoint of molecular weight determination, the magnitude of the sedimentation coefficient alone does not suffice because of its dependence upon shape as well as size of the solute. In the limit of zero solute concentration the sedimentation coefficient of a solute, s_A°, is related to molecular parameters by the expression:

$$s_A^\circ = M_A(1 - \bar{v}_A\rho_s)/(Nf_A) \tag{1}$$

where f_A denotes the shape-dependent translational frictional coefficient of the solute with molecular weight M_A and partial specific volume $\bar{v}_A$: ρ_s is the solvent density and N is Avogadro's number. Because the corresponding diffusion coefficient, D_A°, is governed by the magnitude of the translational frictional coefficient according to the expression:

$$D_A^\circ = RT/(Nf_A) \tag{2}$$

where R and T refer to the universal gas constant and absolute temperature respectively, the influence of f_A on the separate magnitudes of the sedimentation and diffusion coefficients disappears from their ratio: specifically,

$$s_A^\circ/D_A^\circ = M_A(1 - \bar{v}_A\rho_s)/(RT) \tag{3}$$

Inasmuch as the solute distribution at sedimentation equilibrium is governed by this ratio, the parameter to emerge from analysis of such distributions is the buoyant molecular weight, $M_A(1 - \bar{v}_A\rho_s)$.

2.1 Procedural details of a sedimentation equilibrium experiment

Sedimentation equilibrium experiments are conducted in a double-sector cell. One sector contains the macromolecular solution and the other the appropriate solvent. Because proteins, nucleic acids, and many polysaccharides bear net charge, the reference sector needs to contain buffer with which the macro-ion is in dialysis equilibrium so that the chemical potential of the macromolecule (the driving force of diffusion) is defined under conditions of constant chemical potential of solvent (1), which then comprises all diffusible components—buffer species, supporting electrolyte, small ligands, etc., as well as water. This dialysis step leads to a situation wherein the concentration of counterions in the macro-molecular solution exceeds their concentration in the reference sector by the product $|Z_A|C_A/2$, where C_A is the molar concentration of solute with net charge Z_A, whereas the non-counterion concentration in the solution is lower by the same factor. Only for an uncharged macromolecule are the concentrations of diffusible ions identical in the solution and solvent sectors.

Various procedures may be used to effect the required distribution of dialysable ions. Of those, the classical procedure of exhaustive dialysis may be avoided by subjecting the macromolecular solution to zonal gel chromatography on a col-umn pre-equilibrated with the buffer to be used in the solvent sector. Alterna-tively, the use of centrifugal ultrafiltration assemblies can achieve the same result. Although dialysis is precluded for a small solute, the condition of dialysis equilibrium can still be achieved by adjusting the composition of solvent in the reference sector to meet the above distribution requirements—a procedure used to investigate the micellization of chlorpromazine by sedimentation equilibrium (2).

A second consideration in the design of an experiment is the length of the solution column to be subjected to sedimentation equilibrium. Inasmuch as the time to attain equilibrium varies inversely with the square of the column length (3), columns larger than 3 mm are rarely used; and very short columns (< 1 mm) can be used to accelerate the attainment of sedimentation equilibrium (4). Where-as 16–36 hours may be required to achieve the required time-independence of solute distribution in 2–3 mm columns, effective sedimentation equilibrium can be attained (admittedly with decreased accuracy) in less than an hour by de-creasing the column length to below 1 mm (4). The other means of decreasing the duration of an experiment is by resorting to initial overspeeding protocols (5, 6). Inasmuch as equilibrium is, by definition, only reached in the limit of in-finite time, an experiment is deemed to have attained the condition of effective sedimentation equilibrium when distributions recorded several hours apart become time-invariant.

Protocol 1

Sedimentation equilibrium: basic operation

Equipment and reagents

- Ultracentrifuge
- Optical system
- Protein
- Buffer

Method

1 Concentration requirements of the protein: see Chapter 4, *Protocol 1*.

2 Choice of optical system: as Chapter 4, *Protocol 1*. However, with interference optics, the lower limit is ~ 0.5 mg/ml (as opposed to ~ 0.1 mg/ml for simple boundary identification with sedimentation velocity) with the maximum path length cell (12 mm) available in the XL-I centrifuge. (A 2.5-fold lower concentration is permissible with the 30 mm path length cells that can be used in the Model E.) Similarly with UV absorption optics a slightly higher loading concentration (compared with sedimentation velocity) of ~ 0.3 absorbance units should be used. For higher concentrations (> 5 mg/ml for interference optics or > 1.4 absorbance units) use shorter path length cells.

3 Choice of appropriate buffer/solvent. As Chapter 4, *Protocol 1*. For charged macromolecular systems, dialyse solutions against the reference buffer before analysis. Alternatively, employ gel chromatography to achieve dialysis equilibrium (see above).

4 Loading the solutions into the cell. As with sedimentation velocity, double sector cells need to be used. However, solution columns should be shorter to keep the time to reach equilibrium down to acceptable levels. For a 12 mm optical path length cell, a loading volume of 0.1 ml will give a ~ 0.25 cm solution column. Equilibrium is normally attained after ~ 12 h. In the ultra-short column method (4), solution columns of as little as 0.7 mm (~ 0.02 ml) can attain equilibrium within a few hours. The user may also wish to use a multichannel centrepiece in the cell(s) (see Chapter 4, *Figure 1*). These permit three or more solution/solvent pairs. Although they are generally unsuitable for sedimentation velocity work (because of an upper speed limit of ~ 40 000 r.p.m.) they are generally ideal for sedimentation equilibrium. However, because of the non-sector shape of the channels, the use of an inert fluorocarbon oil to give a 'false bottom' in each channel is recommended, although the 'intertness' should be checked beforehand.

5 Choose the appropriate temperature: as in Chapter 4, *Protocol 1*.

6 Speeds are considerably lower than speeds used for velocity sedimentation, by a factor of 2.5–3, unless the 'meniscus depletion' method is being used (about twofold lower compared with sedimentation velocity). Thus for ovalbumin ($M \sim 45\,000$) a regular low speed equilibrium experiment would be conducted at 15 000–20 000 r.p.m., whereas a meniscus depletion experiment would be run at 25 000–30 000

Protocol 1 continued

r.p.m. If meniscus depletion is being attempted, familiarize yourself carefully with its limitations (17, 18, 61). If the regular low- or intermediate speed method is being used, the meniscus concentration needs to be found either by simple extrapolation for UV absorbance optics, or by more sophisticated procedures for interference optics (see later). For schlieren optics (yielding $M_{z,app}$), no such determination is required. The larger the redistribution of solute concentration in the centrifuge cell, the greater is the accuracy of the result. However, attention should be paid to possible loss of optical registration at or near the cell base if too high a speed is chosen. Where possible, two or three equilibrium speeds should be chosen, although this can extend the length of an experiment to several days: care needs to be taken over protein stability.

7 Check for equilibrium by comparing scans/traces recorded several hours apart. Then perform a baseline determination (for UV absorption) by overspeeding (caution required with multichannel cells) and sedimenting all macromolecular solute before recording the residual absorbance. Where this is not possible—namely for smaller proteins (M below about 10 000) where the equilibrium speed is going to be 40 000 r.p.m. or higher—make sure that you have dialysed carefully beforehand and that dialysate is in the reference channel(s). For interference optics a baseline is not necessary, but it may be important to perform a 'blank' correction to correct for window distortion: this is achieved by either:

   (a) Stopping the run, agitating the cell to uniformly redistribute the solute, and returning to the equilibrium speed used before recording a scan immediately.

   (b) Stopping the run, removing the solution and reference solvent (without dismantling or loosening the torque on the cell buttress ring), flushing with water, drying with a current of air, refilling with water in both reference and solution sectors (to the same level as the equilibrium experiment), and then returning to the equilibrium speed used for an immediate scan. These methods are discussed in ref. 62.

8 Evaluate the partial specific volume of the protein (and any macromolecular ligand) using the programme *SEDNTERP* or by densimetry (see Chapter 4, *Protocol 1*).

9 Choose the appropriate software (*Protocol 2*) for analysis.

2.2 Extraction of the molecular weight of a single solute

A sedimentation equilibrium distribution comprises a relatively featureless, monotonic increase in solute concentration, c_A, with radial distance from the air–liquid meniscus (r_a) to the bottom (r_b) of the cell (*Figure 1*). Depending upon whether the absorbance or interference optical system of the Beckman XL-I ultracentrifuge is used to record the distribution, the ordinate is expressed as an absorbance at a given wavelength, $A_\lambda(r)$, or a Rayleigh fringe number, $J(r)$, both being directly proportional to the corresponding solute concentration, $c_A(r)$.
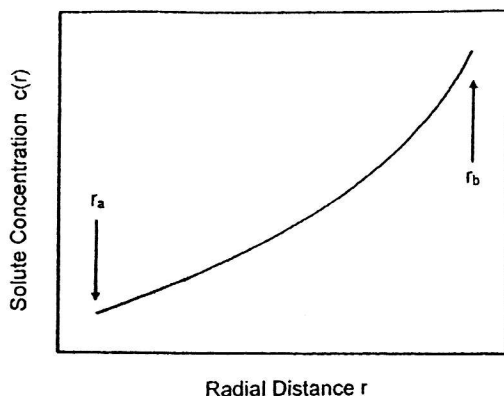
Figure 1 Schematic representation of the concentration distribution in a sedimentation equilibrium experiment on a solution with radial extremities at r_a and r_b.

Sedimentation equilibrium was initially considered in terms of the balance between the sedimentation and diffusional migration processes (7); but it was then realized that the results from such experiments were amenable to rigorous thermodynamic analysis (8, 9). Consequently, even though the experimental record is in terms of solute concentration as a function of radial distance, the distribution of a single solute at sedimentation equilibrium is defined in terms of thermodynamic activity, z_A, and the relationship (10, 11):

$$z_A(r) = z_A(r_F)\exp[M_A(1 - \bar{v}_A\rho_s)\, \omega^2(r^2 - r_F^2)/(2RT)] \qquad [4]$$

In this expression the thermodynamic activity at any given radial distance r is related to its activity at a chosen reference radial distance r_F by an exponential term involving the buoyant molecular weight, the square of the angular velocity (ω) and the difference between the squares of the two radial distances: $M_A(1 - \bar{v}_A\rho_s)\,\omega^2/(2RT)$ is a combination of parameters termed the reduced molecular weight. Such provision of information on the thermodynamic activity of solute is extremely important from the viewpoint of incorporating rigorous allowance for effects of thermodynamic non-ideality into the analysis of sedimentation equilibrium distributions (12–15). However, most studies are performed under conditions approaching thermodynamic ideality; and we therefore simplify presentation of the analysis by considering that the weight-concentrations of solute, $c_A(r)$ and $c_A(r_F)$, may be substituted for $z_A(r)$ and $z_A(r_F)$ respectively in the above expression. From the logarithmic form of *Equation 4* written in those terms it is evident that:

$$M_A(1 - \bar{v}_A\rho_s) = (2RT/\omega^2)\, d[\ln c_A(r)]/dr^2 \qquad [5]$$

which allows the buoyant molecular weight to be determined from the slope of the dependence of the natural logarithm of the concentration upon the square of radial distance. Examples of molecular weight measurement by direct analysis of a sedimentation equilibrium distribution (*Equation 4*) and by means of the
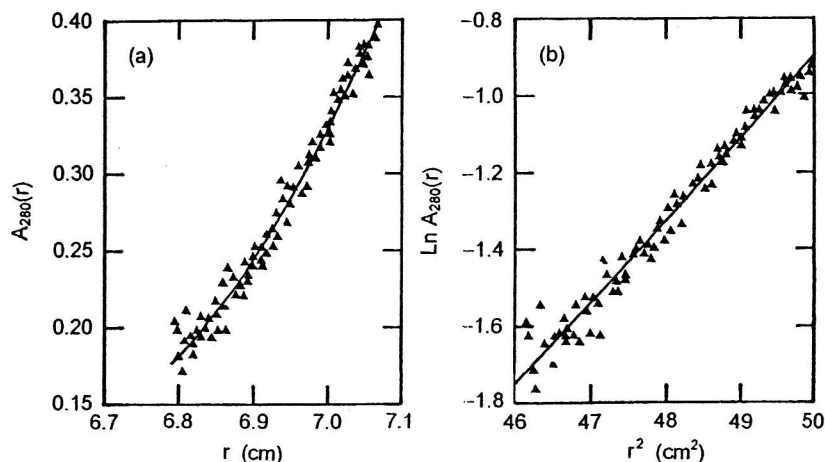
Figure 2 Use of the absorption optical system of the Beckman XL-I ultracentrifuge to determine the buoyant molecular weight of ovalbumin (pH 4.59, $I = 0.16$) by sedimentation equilibrium at 9000 r.p.m. and 20 °C. (a) Absorbance distribution at 280 nm and the best-fit description, $M_A(1 - \bar{v}_A \rho_s) = (11.6 \pm 0.4)$, in terms of *Equation 4* with $r_F = 7.000$ cm. (b) Corresponding analysis of the same distribution according to *Equation 5*, together with the best-fit relationship, $M_A(1 - v_{A\rho s}) = (11.6 \pm 0.4)$, obtained by linear regression analysis.

logarithmic transform (*Equation 5*) are presented in *Figures 2a* and *2b* respectively, which refer to results obtained with the absorption optical system.

Direct application of *Equations 4* and *5* to sedimentation equilibrium distributions recorded by means of the Rayleigh interference optical system is precluded by the fact that the ordinate of the distribution is recorded refractometrically in terms of the difference between the solute concentration at radial distance r and that at the air–liquid meniscus, r_a. This concentration difference is expressed in terms of Rayleigh fringes $j(r)$, where 3.33 fringes corresponds to a concentration difference of 1 mg/ml for proteins (16). $J(r)$, the number of fringes corresponding to the solute concentration $c_A(r)$ must therefore be obtained from the expression:

$$J(r) = J(r_a) + j(r) \qquad [6]$$

which clearly requires knowledge of $J(r_a)$, the refractive index counterpart of $c_A(r_a)$, the solute concentration at the air–liquid meniscus.

An elegant means of overcoming the need to measure $J(r_a)$ is the selection of an angular velocity that ensures a value of essentially zero for the solute concentration at the meniscus (*Figure 3a*), whereupon $J(r) \approx j(r)$. Such practice forms the basis of the very popular high-speed or meniscus-depletion variant of sedimentation equilibrium (17). However, this obvious advantage of the high-speed technique is accomplished at the expense of the range of r over which the radial dependence of $J(r)$ can be used; and hence of the inherent accuracy of the molecular weight measurement. Greater accuracy is attainable from distributions obtained by the low-speed sedimentation equilibrium technique (3) because
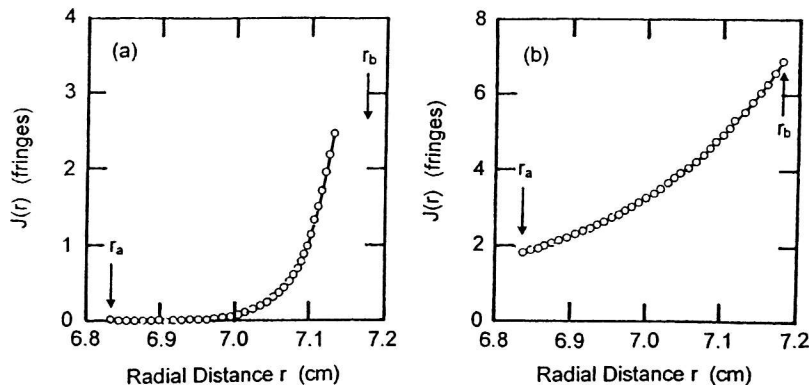
Figure 3 Use of the Rayleigh interference optical system to record sedimentation equilibrium distributions for α-chymotrypsin. (a) Distribution obtained by subjecting an enzyme solution (pH 4.1, *I* 0.08) to centrifugation at 34 000 r.p.m. to achieve solute depletion at the meniscus. (b) Distribution from a sample of α-chymotrypsin (pH 3.9, *I* 0.20) spun at 14 000 r.p.m.

of the ability to analyse the entire distribution (*Figure 3b*). However, its use is conditional upon the measurement of $J(r_a)$ to allow the calculation of $J(r)$ from $j(r)$ via *Equation 6*.

Various methods are available for the determination of $J(r_a)$. In the 'intercept over slope' procedure (18) which has been incorporated in the program '*MSTARI*' for molecular weight analysis from interference optical records (19) the fundamental differential equation of sedimentation equilibrium is manipulated to yield the expression:

$$2RT\,j(r)/[M^*(r)\,(1 - \bar{v}_A\rho_s)\,\omega^2] = J(r_a)\,(r^2 - r_a^2) + 2\int_{r_a}^{r} [r\,j(r)]dr \qquad [7]$$

where $M^*(r)$ is an operational point-average molecular weight at radial distance r: {under thermodynamically ideal conditions for a single solute, $M^*(r) = M_A$ for all r: other useful identities for heterogeneous and non-ideal systems are that $M^*(r_a) = M_{w,app}(r_a)$ and $M^*(r_b) = M_{w,app}$ for the whole distribution (i.e. from meniscus to cell base) in the ultracentrifuge cell (18)}. Rearrangement of *Equation 7* to the form:

$$j(r)/\,(r^2 - r_a^2) = J(r_a)M^*(r)\,(1 - \bar{v}_A\rho_s)\,\omega^2/(2RT)$$
$$+ [M^*(1 - \bar{v}_A\rho_s)\,\omega^2/\{2RT(r^2 - r_a^2)\}]\int_{r_a}^{r} [r\,j(r)]dr \qquad [8]$$

shows that the dependence of $j(r)/(r^2 - r_a^2)$ upon $[\int\{r\,j(r)\}dr]/(r^2 - r_a^2)$ has an ordinate intercept of $J(r_a)M^*(r_a)\,(1 - \bar{v}_A\rho_s)\,\omega^2/(2RT)$ and a limiting slope, as $r \to r_a$, of $M^*(r_a)\,(1 - \bar{v}_A\rho_s)\,\omega^2/(RT)$. The ratio of the ordinate intercept to the limiting slope eliminates $M^*(r_a)$ and is just $J(r_a)/2$. The practical disadvantage of this procedure is that the *limiting slope* is required near the meniscus: data near the meniscus can be notoriously noisy because of the small fringe increments: this problem can be partly obviated by multiple sampling of data sets for a range of radial positions and extrapolating estimated $J(r_a)$ values to $r \to r_a$ (19). Of course

once $J(r_a)$ has been found in this way, an estimate for $M^*(r_a) = M_{w,app}(r_a)$ can be obtained from the slope.

Provided that the entire sedimentation equilibrium distribution is resolved, the problems of extrapolation procedure to obtain $J_a(r)$ can be obviated by performing the integration in *Equations 7* and *8* over the entire range of the distribution, r_a to r_b (the cell base), and invoking the mass conservation requirement that:

$$J_o(r_b^2 - r_a^2) = 2 \int_{r_a}^{r_b} [r\{J(r_a) + j(r)\}]dr = \int_{r_a}^{r_b} [J(r_a) + j(r)]dr^2 \qquad [9]$$

where J_o is the number of Rayleigh fringes observed by forming a boundary between solvent and the loaded solute solution in a separate experiment with a synthetic boundary cell. It then follows that:

$$J(r_a) = [J_o(r_b^2 - r_a^2) - \int_{r_a}^{r_b} j(r)dr^2]/(r_b^2 - r_a^2) \qquad [10]$$

The integration required for the application of this procedure is incorporated into the *MSTAR* program (19) referred to in *Protocol 2*, which allows for revision of the $J(r_a)$ value on the basis of the J_o value thereby deduced (20). It should be noted that mass conservation arguments may also be used to yield an equivalent expression for $J(r_a)$, namely (21):

$$J(r_a) = J_o - [j(r_b)r_b^2 - \int_{r_a}^{r_b} r^2 dj]/ (r_b^2 - r_a^2) \qquad [11]$$

An alternative procedure for determining a model-independent value of $J_a(r)$ entails location of the hinge-point r_h, the radial distance where the solute concentration may be identified with the loading concentration, i.e. the point where $J(r) = J_o$. In current-generation ultracentrifuges the adoption of this procedure relies upon concurrent use of the absorption optical system to record not only the equilibrium distribution but also the distribution immediately after attainment of rotor speed, when $c_A(r)$ is the loading concentration for all r (22). After ascertaining r_h from the intersection point of the two absorbance distributions, the magnitude of $J(r_a)$ is obtained as $J_o - j(r_h)$, whereupon the absolute fringe distribution, $J(r)$ versus r, is again determined from *Equation 6*.

Protocol 2

Sedimentation equilibrium: software

1   Choose first of all a molecular weight program that does not assume a model (monomer, ideal, associating etc.). One such programme is *MSTAR* (19) with two versions: *MSTARA* for UV absorption optics, *MSTARI* for interference optics (a new version *MSTARS* is being constructed for schlieren optics). *MSTAR* works out, amongst other things (i) the (apparent weight) average molecular weight $M_{w,app}$ over the whole distribution of solute in the centrifuge cell (from meniscus r_a to base r_b) and (ii) the (apparent) point weight-average molecular weight $M_{w,app}(r)$ as a function of radial position, r (or the equivalent local concentration $c(r)$. (N.B. If the ultrashort-column

Protocol 2 continued

technique is used it will be difficult to obtain reliable point average data.) The difference between the value of $M_{w(app)}$, recorded over a range of loading concentration and the monomer molecular weight M_1 (from sequence or MALDI mass spectrometry), should give an idea of the presence of protein–macromolecule interactions, and the stoichiometry. Any increase in $M_{w,app}(r)$ vs $c(r)$ should give an additional indication of protein–macromolecular ligand interaction phenomena. $M_{z,app}(r)$ and $M_{z,app}(r)$ data can also be obtained from absorption or interference records (consult the help file for instructions), but reliable data of this sort may not be achievable with UV absorption and is difficult with interference optics because it requires a double mathematical differentiation of the raw concentration data—and each successive differentiation amplifies noise): if $M_{z,app}$ data is required, it is better to use schlieren optics and to consult an advanced user. (The purpose of determining both M_z and M_w is that the ratio M_z/M_w is a useful indicator of heterogeneity.)

2   The routines described in step 1 are based on the extraction of apparent molecular weight (i.e. not corrected for non-ideality). For non-interacting systems non-ideality is either negligible at low concentration (for proteins, usually < 0.5 mg/ml) or is eliminated by extrapolation of $M_{w,app}$ or $M_{w,app}(r)$ to zero concentration. However, care has to be exercised with interacting systems because the extrapolation to zero concentration favours the dissociated state (depending on the reaction strength).

3   If a protein–macromolecular interaction has been identified (using e.g. step 1) then use a program specifically designed for the analysis of interacting systems: for (i) checking the stoichiometry of an interaction, (ii) estimating interaction constants X_i (in g/l) or K_i (in l/mol). Three examples are *ASSOC4* provided by Beckman (64), *NONLIN* (65), and *PSI* (66). *ASSOC4* and *NONLIN* are based on direct analysis of the $c(r)$ vs r data (essentially a truncated form of *Equation 14*). *NONLIN* also permits 'global analysis' in the sense of incorporating multiple sets of data recorded at *different speeds* or *different loading concentrations* in the analysis. Both the Beckman software and *NONLIN* permit the second thermodynamic virial coefficient to be entered if known: this can be predicted from knowledge of the triaxial molecular dimensions, hydration and charge properties (67). However, floating this parameter as a variable to extract association constants is not recommended (see Sections 3.2 and 4.1.2). *PSI* (based on *Equation 24*) allows for the use of arbitrary reference points as opposed to the meniscus (where the data is the least reliable), and permits 'global' analysis in the sense of different species recorded using different optical systems. It is essentially a model independent version of an earlier programme called *OMEGA* (19) based on the omega function (*Equations 15* and *16*). *PSI* also facilitates incorporation of non-ideality and, conversely for single solute systems, provides a means for estimating the second thermodynamic virial coefficient.

2.3 Extraction of point average molecular weights for interacting systems

In a sedimentation equilibrium study of the simplest acceptor–ligand system (A + B $\longleftrightarrow$ C) the solute distribution of each species is described by *Equation 4* written for that specific species, together with the additional restriction that the thermodynamic activities (concentrations for an ideal system) of the two reactants and complex must comply with the law of mass action for the equilibrium reaction (23, 24). From the viewpoint of molecular weight determination, any single estimate must clearly be an average value that takes into account the proportion as well as the molecular weight of each species. Furthermore, the relative composition varies with radial distance (*Figure 4a*) and hence the average molecular weight also reflects that variation, which is manifested (*Figure 4b*) as curvilinearity in the plot of total concentration $c(r)$ (—) according to *Equation 5*. The traditional molecular weight approach to ultracentrifugal analysis of such a system thus requires delineation of the radial dependence of the weight-average molecular weight, $\bar{M}_w(r)$, which is governed by the expressions:

$$\bar{M}_w(r) = [c_A(r)M_A + c_B(r)M_B + c_C(r)M_C]/\bar{c}(r) \qquad [12a]$$

$$\bar{c}(r) = c_A(r) + c_B(r) + c_C(r) \qquad [12b]$$

$$c_C(r) = X_{AB}c_A(r)c_B(r) \qquad [12c]$$

where X_{AB}, the association equilibrium constant with species concentrations (c_i) expressed in g/litre, is related to its more traditional molar counterpart, K_{AB}, by:

$$X = K_{AB}M_C/(M_AM_B) \qquad [12d]$$

Larger changes in average molecular weight are observed when the optical system allows delineation of a constituent distribution, say $\bar{c}_B(r) = c_B(r) + (M_B/M_C)c_C(r)$, rather than (or as well as) the distribution in terms of total concentration, $\bar{c}(r)$. This gives rise to a more curvilinear plot for the dependence of ln $[\bar{c}_B(r)]$ upon square of the radial distance (– – –, *Figure 4b*); and reflects the fact that the constituent weight-average molecular weight, $\bar{M}_B(r)$ is given by the relationship:

$$\bar{M}_B(r) = [c_B(r) + c_C(r)]M_B/\bar{c}_B(r) \qquad [12e]$$

Methods have certainly been developed (18, 25–28) for determining the required point-average molecular weights $\bar{M}_w(r)$—a task that amounts to defining the slope of the tangent to the curvilinear plot in *Figure 4b* for each value of r. Furthermore, the analysis of the consequent $[\bar{M}_w(r), \bar{c}(r)]$ or $[\bar{M}_B(r), \bar{c}_B(r)]$ data has also been the subject of theoretical deliberations (23, 24), but the method does not seem to have been put into practice. It transpires that direct analysis of the sedimentation equilibrium distribution affords a simpler approach which avoids the undesirable magnification of experimental error associated with differentiation to obtain d[ln $\bar{c}(r)$]/dr^2 or d[ln $\bar{c}_B(r)$]/dr^2 at each radial distance.
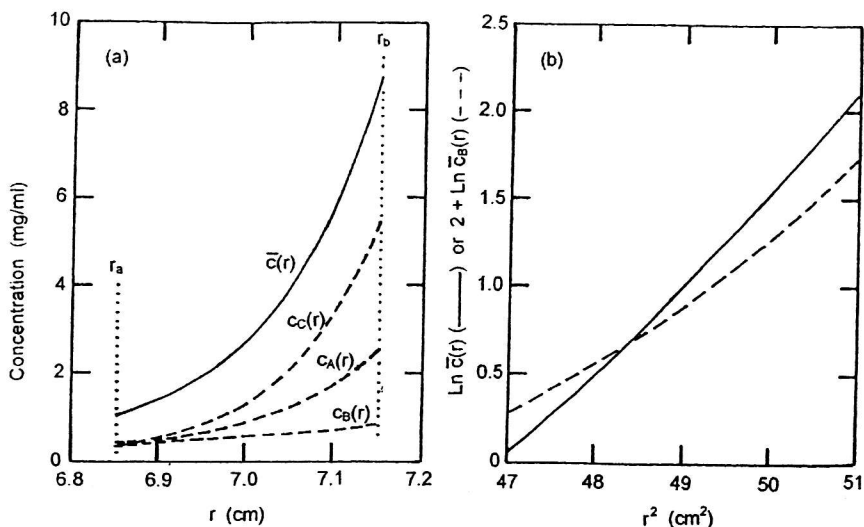
115

Figure 4 Characterization of an acceptor–ligand interaction by molecular weight analysis of a sedimentation equilibrium distribution. (a) Concentration distributions from a simulated sedimentation equilibrium experiment (12 000 r.p.m., 20 °C) based on *Equation 4* and the following set of parameters for a 1:1 interaction between acceptor and ligand with respective molecular weights of 60 000 and 20 000 (buoyant molecular weights of 15.6 and 5.2): r_a = 6.85 cm, r_b = 7.15 cm, r_F = 7.00 cm; $C_A(r_a)$ = 5 μM, $C_B(r_a)$ = 20 μM, K_{AB} = 40 000 M^{-1}. Broken lines signify the simulated distributions for the indicated species, whereas the solid line is the distribution in terms of total solute concentration $\bar{c}(r)$. (b) Analysis of the distributions in terms of total solute concentration $\bar{c}(r)$ and ligand constituent concentration $\bar{c}_B(r)$ according to *Equation 5*.

2.4 Direct curve-fitting of concentration distributions

For a reversible interaction involving complex formation between a multivalent acceptor A and a univalent ligand B there are only two independent sediment-ation equilibrium distributions to consider. That for the A component, which includes acceptor contributing to the various complexes AB$_i$ as well as free reactant, is given by:

$$\bar{C}_A(r) = C_A(r) + K_{AB}C_A(r)C_B(r) + K_{AB_2}C_A(r)[C_B(r)]^2 + \ldots \qquad [13a]$$

whereas the sedimentation equilibrium distribution for the ligand component is described by:

$$\bar{C}_B(r) = C_B(r) + K_{AB}C_A(r)C_B(r) + 2K_{AB_2}C_A(r)[C_B(r)]^2 + \ldots \qquad [13b]$$

K_{AB} and K_{AB2} are binding constants that describe the combined concentrations of all complexes with a given stoichiometry. Molar concentrations (C_i) have been used to allow expression of the proportions of A and B in the various complexes as simple integers. The condition of sedimentation equilibrium, *Equation 4* with $C_i(r)$ substituted for $z_A(r)$ in an ideal system, is now introduced to allow *Equations 13a* and *13b* to be written in the form:

$$\bar{C}_A(r) = C_A(r_F)\,\psi_A(r) + K_{AB}C_A(r_F)C_B(r_F)\,\psi_A(r)\,\psi_B(r)$$
$$+ K_{AB_2}C_A(r_F)[C_B(r_F)]^2\psi_A(r)[\,\psi_B(r)]^2 + \ldots \qquad [14a]$$

$$\bar{C}_B(r) = C_B(r_F)\,\psi_B(r) + K_{AB}C_A(r_F)C_B(r_F)\,\psi_A(r)\,\psi_B(r)$$
$$+ 2K_{AB_2}C_A(r_F)[C_B(r_F)]^2\psi_A(r)[\,\psi_B(r)]^2 + \ldots \qquad [14b]$$

$$\psi_i(r) = \exp[M_A(1 - \bar{v}_{i\rho s})\,\omega^2(r^2 - r_F^2)/(2RT)]$$
$$i = A, B \qquad [14c]$$

On noting that $\psi_A(r) = [\psi_B(r)]^u$ where $u = [M_A(1 - \bar{v}_A\rho_s)]/[M_B(1 - \bar{v}\rho_s)]$, the right-hand sides of *Equations 14a* and *14b* are discrete multinomials in $\psi_B(r)$, with the coefficients of the series defined in terms of the constant parameters $c_A(r_F)$, $c_B(r_F)$, K_{AB}, K_{AB2}, etc. Furthermore, determination of the buoyant molecular weight, $M_i(1 - \bar{v}_i\rho_s)$, of the two reactants from separate sedimentation equilibrium experiments on each reactant in the absence of the other allows $\psi_B(r)$ to be regarded as the independent variable (22, 29). The extent to which advantage may be taken of direct curve-fitting to *Equation 14* for evaluation of the equilibrium constant(s) and the reference radial concentrations of the two free reactants clearly depends upon the nature and number of sedimentation equilibrium distributions available for analysis.

Inasmuch as the sedimentation equilibrium distributions are recorded optically in the analytical ultracentrifuge, there are several situations that may be encountered. The maximal potential for quantitative analysis of a sedimentation equilibrium experiment pertains when the optical system allows access to the radial distributions of the separate concentrations of acceptor and ligand constituents, $\bar{C}_A(r)$ and $\bar{C}_B(r)$, whereupon the objective of direct curve-fitting is the best description of both distributions in terms of a single set of parameters (30–33). To date this approach has been restricted to the analysis of sedimentation equilibrium distributions recorded at different wavelengths to resolve the separate distributions for the A and B constituents—an approach that relies upon additivity of the absorbances of reactants and complex(es) at each given wave length. It is therefore necessary to demonstrate the validity of this assumption/approximation by recording spectra of mixtures with a range of acceptor/ligand ratios.

Because the Beckman XL-A ultracentrifuge is only equipped with the absorption optical system, the study of interactions such as those between proteins and polysaccharides is disadvantaged in that the only recorded sedimentation equilibrium distribution is in terms of the protein constituent. This situation needs to be accommodated despite a relative lack of information on which to base the quantitative analysis. In similar vein there is a need to consider the circumstance in which the only available sedimentation equilibrium distribution is related to the combined constituent concentrations of acceptor and ligand, $\bar{C}_A(r) + \bar{C}_B(r)$. This situation is the norm in sedimentation equilibrium studies of interactions by means of the interference optical system, but has also been encountered in an XL-A investigation of an interaction between two flavoproteins (34).

The latter two situations are clearly suboptimal from the viewpoint of interpreting quantitatively a sedimentation equilibrium experiment by direct curvefitting of the single distribution that is available. Alternative procedures based on the integrated form of the sedimentation equilibrium expression for a single solute (*Equation 4*) have been devised which illustrate the feasibility of a quantitative analysis even under these adverse circumstances (22, 34).

2.5 Omega and psi analyses of sedimentation equilibrium distributions

A major breakthrough in the interpretation of sedimentation equilibrium distributions for interacting systems was the decision to abandon the use of molecular weight analysis in favour of evaluation of the thermodynamic activity of the smallest species contributing to a sedimentation equilibrium distribution (11, 35, 36). For this purpose the omega function for the smaller (ligand) reactant, $\Omega_B(r)$, was obtained from the Rayleigh sedimentation equilibrium distribution by means of the relationship:

$$\Omega_B(r) = [\bar{c}(r)/\bar{c}(r_F)]\exp[M_B(1 - \bar{v}_B\rho_s)\,\omega^2(r_F^2 - r^2)/\,(2RT)] \qquad [15]$$

where $\bar{c}(r)$ and $\bar{c}(r_F)$ denote the total solute concentrations at the respective radial and reference radial positions. On the grounds that:

$$\lim_{\bar{c}(r)\to 0} \Omega_B(r) = z_B(r_F)M_B/\bar{c}(r_F) \qquad [16]$$

the thermodynamic activity of free ligand at the reference radial position, $z_B(r_F)$, was then obtained from the ordinate intercept of the dependence of $\Omega_B(r)$ upon $\bar{c}(r)$; and the thermodynamic activity of free ligand throughout the distribution determined by applying *Equation 4* (11). Subject to the validity of assumed thermodynamic ideality, each experimentally determined value of $c_B(r)$ could be subtracted from $\bar{c}_B(r)$ to yield a revised concentration distribution, $\bar{c}_A^*(r)$ versus r, with the acceptor the smallest contributor. Repetition of the above steps with the omega function defined as $\Omega_A(r)$ could then be used to yield $c_A(r_F)$ and hence $c_A(r)$ throughout the distribution. As noted at that early stage (35, 36), successive application of the omega procedure to the residual distributions has the potential to define the concentrations of all reactant and product species contributing to the original dependence of $\bar{c}(r)$ upon radial distance; and hence to define the equilibrium constant(s) describing complex formation between acceptor and ligand.

In the event that separate concentration distributions are available for the acceptor and ligand constituents, the same approach can be applied to each of the distributions on the basis of a redefined definition of $\Omega_i(r)$, namely:

$$\Omega_i(r) = [\bar{C}_i(r)/\bar{C}_i(r_F)]\exp[M_i(1 - \bar{v}_i\rho_s)\,\omega^2(r_F^2 - r^2)/\,(2RT)] \qquad [17]$$

to obtain the free acceptor and free ligand activity distributions from the respective sedimentation equilibrium distributions in terms of $\bar{C}_A(r)$ and $\bar{C}_B(r)$. For the ideal case subtraction of each $\bar{C}_i(r)$ from $C_i(r)$ allows access to $C_{AB}(r)$ from the

next round of omega analysis on the residual distributions for acceptor and ligand constituents. Equilibrium constants evaluated under such circumstances should exhibit less experimental error because of the greater amount of information upon which the analysis is based.

A drawback of the omega analysis is the extent of reliance placed upon the accuracy of a curvilinear extrapolation to obtain $C_i(r_F)$ from the ordinate intercept of the dependence of $\Omega_i(r)$ upon $\bar{C}_i(r)$ (*Figure 5a*). Furthermore, the method is open to criticism on the statistical grounds that there is no independent variable. These deficiencies are readily overcome by resorting to the psi function (13–15, 22), which has already been defined in *Equation 14c*. As well as providing the basis for the model-dependent curve-fitting procedure described above, *Equations 14a* and *14b* may be used to evaluate the free concentrations of acceptor and ligand at the reference radial position independently of any model of the interaction. Specifically, division of *Equation 14b* by $\psi_B(r)$ yields the expression:

$$\bar{C}_B(r)/\,\psi_B(r) = C_B(r_F) + K_{AB}C_A(r_F)C_B(r_F)\,\psi_A(r) + ... \qquad [18a]$$

which signifies that the concentration of free ligand at the reference radial position may be obtained as the ordinate intercept of the dependence of $\bar{C}_B(r)/\psi_B(r)$ upon $\psi_A(r)$. This dependence is linear if complex formation is restricted to 1:1 stoichiometry and acceptably curvilinear if higher complexes are formed (*Figure 5b*). Corresponding analysis of the acceptor constituent concentration distribution in terms of the expression:

$$\bar{C}_A(r)/\,\psi_A(r) = C_A(r_F) + K_{AB}C_A(r_F)C_B(r_F)\,\psi_B(r) + ... \qquad [18b]$$

has the potential to yield $C_A(r_F)$ (*Figure 5c*) and hence $C_A(r)$ throughout the distribution. K_{AB}, K_{AB_2}, etc., may therefore be evaluated by curve-fitting the $[\bar{C}_A(r),$
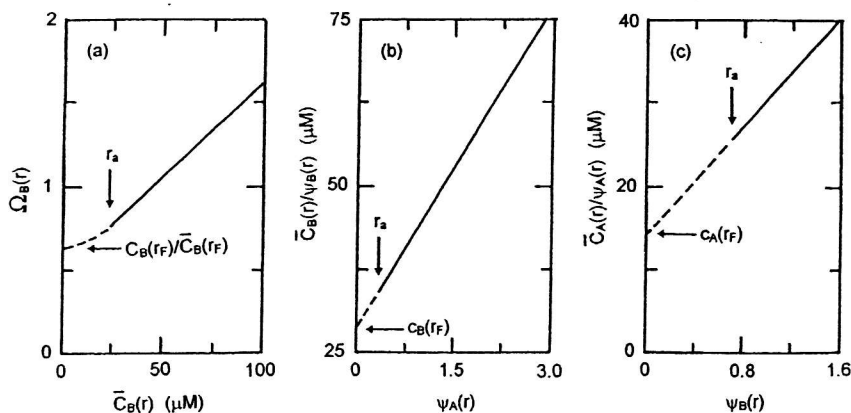

Figure 5 Comparison of the omega and psi procedures for analysis of the sedimentation equilibrium distributions simulated in *Figure 3*. (a) Evaluation of $C_B(r_F)/\bar{C}_B(r_F)$ as the ordinate intercept of the plot of $\bar{C}_B(r)$ data according to *Equation 17* with $r_F = 7.00$ cm. (b) Corresponding psi analysis of the same data according to *Equation 18a* to obtain $C_B(r_F)$ as the ordinate intercept. (c) *PSI* analysis (*Equation 18b*) of the distribution for acceptor constituent to obtain $C_A(r_F)$.

119

$\bar{C}_B(r)$, $C_A(r)$, $C_B(r)$] data set in terms of *Equations 14a* and *14b*. Alternatively, the combination of $C_B(r)$ from analysis of the ligand constituent concentration distribution with the corresponding values of $\bar{C}_B(r)$ and $\bar{C}_A(r)$ allows analysis of the results in conventional binding fashion, namely:

$$\nu\,(r) = [\bar{C}_B(r) - C_B(r)]/\bar{C}_A(r) \tag{19a}$$

$$= \{K_{AB}C_B(r) + 2K_{AB2}[C_B(r)]^2 + ..\}/\{1 + K_{AB}C_B(r) + K_{AB2}[C_B(r)]^2 + ...\} \tag{19b}$$

Such analysis has been used to characterize an electrostatic interaction between ovalbumin and cytochrome c at low ionic strength and neutral pH (21).

Although lacking the sophistication of the direct curve-fitting procedure, the psi analysis does have some advantages from the experimental viewpoint.

(a) In keeping with its predecessor, the omega analysis, the method based on the psi function extracts experimental estimates of the concentration distributions for the free reactants independently of any model of the acceptor–ligand interaction.

(b) $\psi_i(r)$ is a transformed but acceptable independent variable because of the essential absence of uncertainty in the measurement of radial distance.

(c) If desired, complete separation of the dependent ($\bar{C}_B(r)$) from the independent ($\psi_B(r)$) variable can be effected by determining $C_B(r_F)$ as the limiting slope of the dependence of $\bar{C}_B(r)$ upon $\psi_B(r)$ (*Equation 14b*) rather than as the ordinate intercept of the dependence of $\bar{C}_B(r)/\psi_B(r)$ upon $\psi_A(r)$ (*Equation 18a*).

A description of the execution of this procedure is given in *Protocol 3*.

Protocol 3

Characterization of a macromolecular interaction between dissimilar reactants by sedimentation equilibrium

Equipment and reagents

• See *Protocol 1*

Method

1 Evaluate the buoyant molecular mass, $M_1(1 - \bar{v}\rho_s)$, of each reactant (A, B) by sedimentation equilibrium of the individual reactants in the buffer to be used for mixtures thereof (see *Protocol 1*).

2 On the basis of a rough estimate of the binding constant for the acceptor–ligand interaction, prepare a mixture with composition [$\bar{C}_A$, $\bar{C}_B$] that should give rise to an equilibrium mixture with significant concentrations of complex and reactant species.

3 Select a rotor speed for the equilibrium run from the weight-average molecular mass predicted (*Equation 12*) for such an equilibrium mixture.

4 Subject the reaction mixture (150 μl) to centrifugation at the designated rotor

Protocol 3 continued

    speed for 16–28 hours, by which time the solute distribution(s) recorded at 4 hourly intervals should be superimposable. Where possible, use a combination of optical records of the distribution that allows delineation of $\bar{C}_A(r)$ and $\bar{C}_B(r)$.

5 Evaluate $C_B(r)$, the concentration of smaller reactant (ligand) at a selected reference radial position (e.g. column midpoint) from the ordinate intercept of the dependence of $\bar{C}_B(r)/\psi_B(r)$ upon $\psi_A(r)$ (*Equation 18*).

6 Determine $C_B(r) = C_B(r_F)\psi_B(r)$ throughout the entire distribution.

7 Calculate the binding function, $\nu(r)$, from $\bar{C}_A(r)$, $\bar{C}_B(r)$, and $C_B(r)$ for the evaluation of the binding constant(s) via *Equation 19*.

8 In the event that the only solute distribution available is in terms of total solute concentration, $[\bar{C}_A(r) + \bar{C}_B(r)]$, substitute this parameter for $\bar{C}_B(r)$ in step 5 to obtain $C_B(r_F)$ and hence $C_B(r)$ from step 6.

9 Subtract $C_B(r)$ from $[\bar{C}_A(r) + \bar{C}_B(r)]$ to obtain a revised total solute distribution in which A is now the smallest species.

10 Obtain $C_A(r_F)$ from the ordinate intercept of the dependence of $[\bar{C}_A(r) + \bar{C}_B(r) - C_B(r)]/\psi_A(r)$ upon $\psi_{AB}(r)$; and hence $C_A(r) = C_A(r_F))/\psi_A(r)$ throughout the distribution.

11 Refer to refs 22 and 34 for the evaluation of equilibrium constants (K_{AB}, K_{AB_2}, etc.) from the $[\bar{C}_A(r), \bar{C}_B(r), C_A(r), C_B(r)]$ data set.

3 Sedimentation equilibrium studies of ligand binding

A major limitation of *sedimentation velocity* procedures (as described in the previous chapter) for the characterization of acceptor–ligand interactions is the need to adopt a hydrodynamic model of any postulated complex in order to assign a magnitude to s_{AB}. Inasmuch as the molecular weight of the same complex can be assigned unambiguously on the basis of M_A, M_B and the postulated stoichiometry (*i*), the analysis of sedimentation equilibrium distributions has obvious advantages over sedimentation velocity methods for characterizing acceptor–ligand interactions. Apart from an isolated study of the ovalbumin-lysozyme interaction 20 years ago by means of the omega analysis (36), the use of sedimentation equilibrium for the characterization of acceptor–ligand interactions has been restricted to post-1990. By then the advantages of direct analysis of concentration (absorbance) distributions had been realized; and accordingly the use of average molecular weights for such characterization has largely been by-passed.

3.1 Evaluation of the concentration distributions of individual species

To date there have been only three studies in which the characterization of an acceptor–ligand interaction has been based on the extraction of model-

independent concentration distributions for the two free reactants from sedimentation equilibrium experiments on mixtures of the two reactants. Because the inaugural experimental study (36) employed the Rayleigh optical system, it inevitably encountered the least desirable situation where the only information available is in terms of the total solute concentration distribution. A similar situation was encountered in a recent study of the interaction between an electron transferring flavoprotein and trimethylamine dehydrogenase by means of the XL-A absorption optical system (34), both reactants being flavoproteins with comparable spectral characteristics throughout the entire range of accessible ultra-violet and visible wavelengths. In the other study (22) the two reactants, ovalbumin and cytochrome c, were chosen deliberately to illustrate the optimal situation with access to the separate constituent concentration distributions, $\bar{C}_A(r)$ and $\bar{C}_B(r)$.

3.1.1 Analysis of the total concentration distribution

In the characterization of the ovalbumin–lysozyme interaction from Rayleigh optical records of the total concentration distribution (36), the omega analysis (*Equation 15*) was first used to evaluate $c_B(r_F)$ (*Figure 6a*) and hence the concentration distribution of free lysozyme throughout the distribution via *Equation 4*. Subtraction of $c_B(r)$ from $\bar{c}_B(r)$ then led to a revised total distribution, $\bar{c}^*(r)$ versus r, with ovalbumin as the smallest solute species. Repetition of the omega analysis on the revised distribution (*Figure 6b*) then yielded $c_A(r_F)$ and hence $c_A(r)$ throughout the distribution.

A comparable procedure was adopted in a sedimentation equilibrium study (34) of the interaction between an electron transferring flavoprotein (B) and tri-
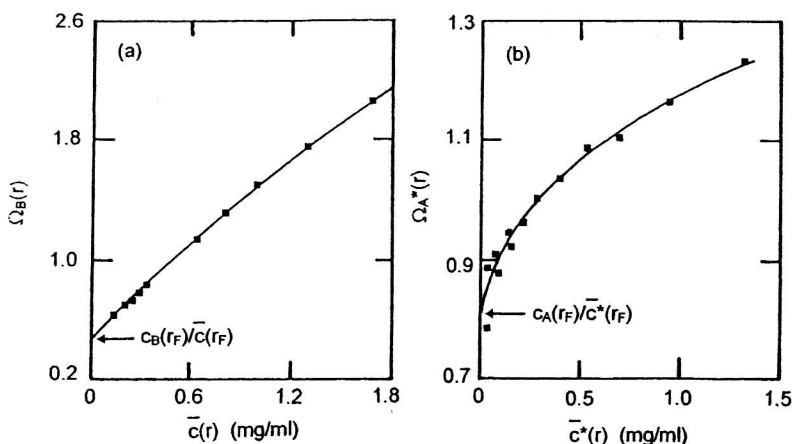

Figure 6 Determination of the free concentrations of lysozyme (B) and ovalbumin (A) by omega analysis of a Rayleigh sedimentation equilibrium distribution for a mixture of the two reactants. (a) Dependence of $\Omega_B(r)$ (*Equation 15*) upon total concentration $\bar{c}(r)$ to obtain $c_B(r_F)$ in a mixture with a total concentration, $\bar{c}(r_F)$, of 0.52 mg/ml. (b) Corresponding dependence of $\Omega_A^*(r)$ residual total concentration $c^*(r)$ to obtain $c_A(r_F)$ at the same reference radial position. Data are taken from ref. 36.
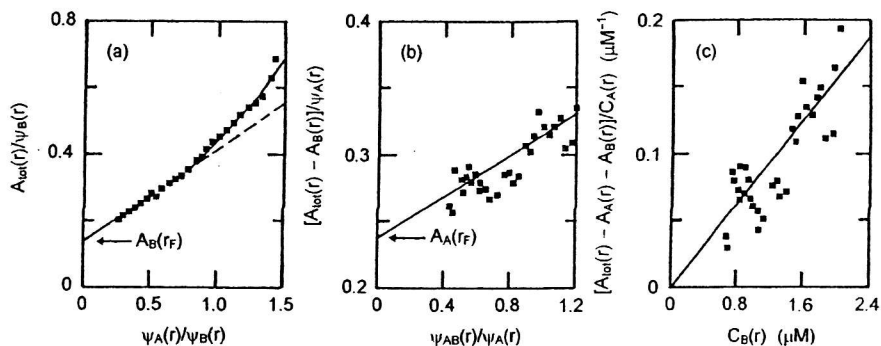
Figure 7 Characterization of the interaction between an electron transferring flavoprotein (B) and trimethylamine dehydrogenase (A) by psi analysis of a sedimentation equilibrium distribution (A_{280}) for a mixture of the two reactants. (a) Determination of $A_B(r_F)$ as the ordinate intercept of the dependence of $A_{tot}(r)/\psi_B(r)$ upon $\psi_A(r)/\psi_B(r)$ for a mixture with $A_{tot}(r_F) = 0.45$. (b) Corresponding plot of the residual total absorbance distribution to obtain $A_A(r_F)$ as the ordinate intercept. (c) Evaluation of the equilibrium constant K_{AB}. Data are taken from ref. 34.

methylamine dehydrogenase (A) except that psi rather than the omega function was used to evaluate absorbances corresponding to $c_B(r_F)$ and $c_A(r_F)$ (*Figures 7a* and *7b*). The equilibrium constant, K_{AB}, was then obtained by plotting the residual absorbance at 280 nm divided by the free concentration of dehydrogenase as a function of free electron transferring flavoprotein (*Figure 7c*). Because trimethyl-amine dehydrogenase (a dimer) possesses two sites for electron transferring flavoprotein, the slope of *Figure 7c* (K_{AB} multiplied by the molar absorption co-efficient of complex) almost certainly defines $2k_{AB}$, where k_{AB} is the intrinsic binding constant (37). In that regard the essentially linear form of *Figure 7b* signifies the contribution of essentially a single species to the residual absorb-ance (see *Figure 5*), whereupon the contribution of AB_2 must be negligible—an inference supported by the essentially linear nature of *Figure 7c*.

3.1.2 Analysis of separate constituent concentration distributions

As noted above, the only other attempt to extract a reactant concentration dis-tribution from sedimentation equilibrium results for an acceptor–ligand system (22) involved a study of the electrostatic interaction between cytochrome c (B) and ovalbumin (A) at low ionic strength (pH 6.3, $I = 0.03$). *Figure 8a* presents sedi-mentation equilibrium distributions recorded at 410 and 280 nm for a mixture of ovalbumin and cytochrome c that had been centrifuged to equilibrium at 15 000 r.p.m. and 20 °C. Because the cytochrome c constituent is the only con-tributor to the distribution recorded at 410 nm, the radial dependence of $\bar{C}_B(r)$ is readily obtained as $A_{410}(r)$ divided by the molar absorption coefficient of cyto-chrome c at that wavelength (*Figure 8b*). Knowledge of the relative magnitudes of the molar absorption coefficients of cytochrome c at 280 and 410 nm then allows calculation of the contribution of $\bar{C}_B(r)$ to $A_{280}(r)$, whereupon $\bar{C}_A(r)$ is obtained from the residual absorbance at each radial distance (*Figure 8b*).
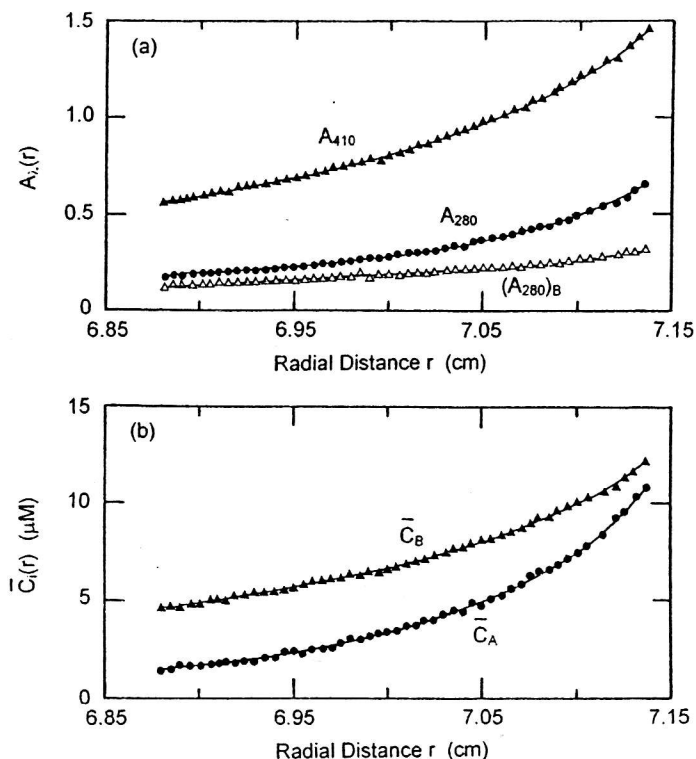
Figure 8 Sedimentation equilibrium distributions at 15 000 r.p.m. and 20 °C for a mixture of ovalbumin (A) and cytochrome *c* (B). (a) Distributions in terms of absorbances at 410 and 280 nm, together with the estimated contribution of the cytochrome *c* constituent to the absorbance at 280 nm. (b) Constituent concentration distributions for the two components. Data are taken from ref. 22.

Analysis of the $\bar{C}_B(r)$ distribution in terms of *Equation 18a* is presented in *Figure 9a*, where the essentially linear dependence of $\bar{C}_B(r)/\psi_B(r)$ upon $\psi_A(r)$ indicates the dominance of 1:1 complex formation between cytochrome *c* and ovalbumin under these conditions. Substitution of the value of $C_B(r_F)$ obtained from the ordinate intercept into *Equation 4* again allows calculation of $C_B(r)$ throughout the distribution, and hence of the binding function $\nu(r)$ via *Equation 19*. Results from a series of sedimentation equilibrium experiments on acceptor–ligand mixtures are presented as a binding curve in *Figure 9b*, which signifies a binding constant K_{AB} (*Equation 19b*) of (60 000 ± 2000) M^{-1} for 1:1 complex formation between ovalbumin and cytochrome *c* (22).

3.2 Direct modelling of sedimentation equilibrium distributions

The majority of studies of acceptor–ligand interactions by sedimentation equilibrium have employed direct curve-fitting of absorbance distributions at two or more wavelengths in order to determine the binding constant for 1:1 inter-
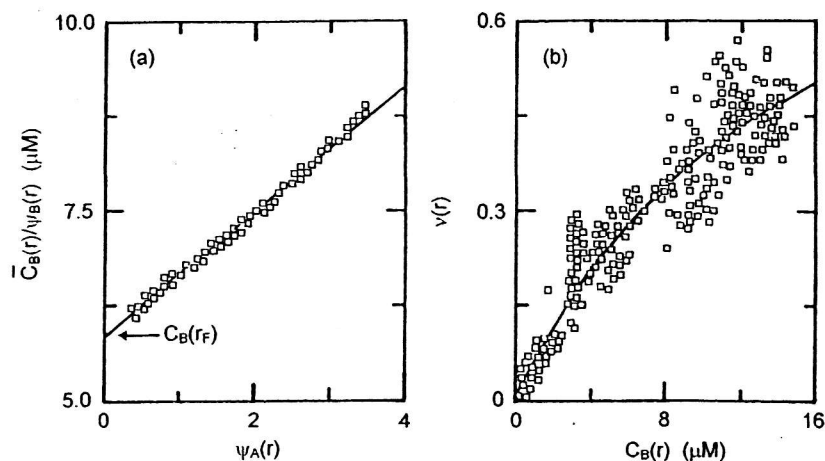
Figure 9 Characterization of the interaction between ovalbumin (A) and cytochrome c (B), pH 6.3, $I = 0.03$, by sedimentation equilibrium. (a) Evaluation of $C_B(r_F)$ at the reference radial position (7.000 cm) by psi analysis (*Equation 18a*). (b) Binding curve, together with the best-fit description ($p = 1$, $K_{AB} = 60\,000$ M^{-1}) in terms of *Equation 19b*. Data are taken from ref. 22.

action (30–33) and for interactions with greater stoichiometry (38). Software programs are supplied with the Beckman instrument to facilitate such endeavours, which amount to curve-fitting of the distributions to *Equations 14a* and *14b* (truncated at the second term on the right-hand side for 1:1 complex formation) or their equivalents in terms of absorbances and molar absorption coefficients. The steps involved in the characterization of an acceptor–ligand interaction by direct curve-fitting are outlined in a recent discussion (39) of the characterization of heterogeneous associations. Furthermore, that investigation (39) extends the analysis by incorporating into *Equations 14a* and *14b* the capacity to make rigorous allowance for the effects of thermodynamic non-ideality on the statistical-mechanical basis of excluded volume.

Although more elegant and potentially far more accurate than the procedures described in the previous two sections, the direct curve-fitting procedures are, of course, model-dependent from the outset. Such model-dependence poses no great problem when the experimenter is certain of the reaction stoichiometry, but it is rather disconcerting to find $C_A(r_F)$ and $C_B(r_F)$ undergoing variation as the result of including extra terms in *Equations 14a* and *14b* to encompass a range of possible reaction stoichiometries. Despite the greater inaccuracy of the procedures illustrated in *Figures 6–9* because of promulgated errors in $C_A(r)$ (*Figures 6* and *7*) or $\bar{C}_B(r) - C_B(r)$ (*Figure 9*) as the result of uncertainty inherent in the estimates of $C_B(r)$, those methods do have the advantage of being model-independent until the final step. They may therefore be preferable for delineating the model of the interaction, which is based on fitting the experimental data $[\bar{C}_A(r), \bar{C}_B(r)]$ to specified expressions (*Equations 14a* and *14b*) in the two model-independent variables $C_A(r)$ and $C_B(r)$. Subsequent refinement of the characterization in terms of

125

affinity (K_{AB}, etc.) may then well ensue from direct curve-fitting of the results in terms of the model emanating from that first analysis.

4 Ligand perturbation of acceptor self-association

The major emphasis in ultracentrifugal studies of interacting systems has undoubtedly been the characterization of protein self-association (11, 13, 27, 40–48). In the present context advantage has been taken of that experience to delineate binding parameters for the interactions of small ligands with the various oligomeric states of an acceptor (49–56). Introduction of the concepts involved in these preferential binding studies is predicated upon an understanding of the characterization of acceptor self-association by sedimentation equilibrium—a topic that is therefore considered first.

4.1 Characterization of acceptor self-association by sedimentation equilibrium

Because studies of solute self-association heralded the introduction of sedimentation equilibrium for the characterization of macromolecular interactions, the field was developed initially in the context of molecular weight measurement. We therefore begin with a discussion of that approach, which has, however, been superseded by direct analysis of the sedimentation equilibrium distributions for a self-associating solute.

4.1.1 Analysis of weight-average molecular weights

The concentration-dependence of weight-average molecular weight deduced from separate sedimentation equilibrium distributions for lysozyme (43) are presented in *Figure 10a*. From this information we now need to manipulate the results to obtain f_1, the weight-fraction of solute in monomeric state. By combining the expression (57, 58):

$$\bar{M}_A/M_1 = \mathrm{d}(\ln \bar{c}_A)/\mathrm{d}(\ln C_1) \qquad [20]$$

with that for the weight-fraction of monomer:

$$f_1 = c_1/\bar{c}_A = M_1 C_1/\bar{c}_A \qquad [21]$$

where C_1 is the molar concentration of monomer with molecular weight M_1, it follows that:

$$\ln f_1 = \int_0^{\bar{c}_A} \{[(M_1/\bar{M}_A) - 1]/\bar{c}_A\}\mathrm{d}\bar{c}_A \qquad [22]$$

A plot of the dependence of $\{[(M_1/\bar{M}_A) - 1]/\bar{c}_A$ upon $\bar{c}_A$ (*Figure 10b*) has the potential to provide their inter-relationship as the precursor of numerical integration to obtain the weight-fraction of monomer from *Equation 22*. Finally, curve-fitting of the dependence of total concentration, c_A, upon monomer concentration, $c_1 = f_1\bar{c}_A$, to the expression:

$$\bar{c}_A = c_1 + X_2 c_1^2 + X_3 c_1^3 + \ldots \qquad [23]$$
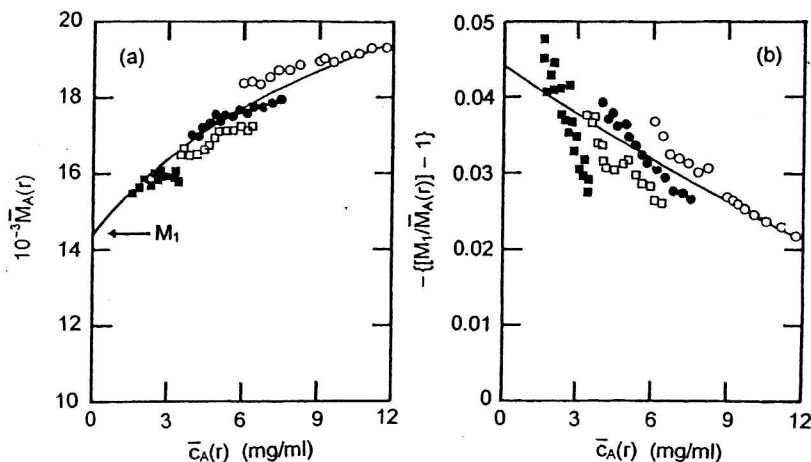
Figure 10 Characterization of solute self-association by analysis of sedimentation equilibrium distributions in terms of weight-average molecular weight. (a) Concentration dependence of $\bar{M}_A(r)$ obtained from four sedimentation equilibrium experiments on lysozyme (pH 6.7, $I = 0.17$, 15 °C), the data being taken from ref. 43. (b) Replot of the results for evaluation of the weight-fraction of monomer via *Equation 22*.

is used to obtain the various equilibrium constants X_i (litre^{i-1} g^{1-i}) describing the formation of *i*-mer from monomer.

    A shortcoming of this approach is the differentiation of the sedimentation equilibrium distributions, $\bar{c}_A(r)$ versus r, to obtain $\bar{M}_A(r)$ as $d[\ln\bar{c}_A(r)]/dr^2$ at radial distance r. This procedure magnifies the uncertainty inherent in the experimental distribution, and thereby renders very difficult the delineation of the relationship to be integrated in *Equation 22* (*Figure 10*). Furthermore, the approach is circular in the sense that the molecular weight data obtained by differentiation are then re-integrated to obtain f_1, the weight-fraction of monomer. For over 20 years such use of molecular weight measurements has been rendered redundant by the realization that direct analysis of sedimentation equilibrium distributions affords a simpler and more accurate means of characterizing solute self-association (11, 13, 39, 59).

4.1.2 Direct analysis of sedimentation equilibrium distributions

By analogy with *Equations 13* and *14*, a more direct approach to the analysis of sedimentation equilibrium distributions reflecting solute self-association is to incorporate the psi function (*Equation 14c*) for monomer into *Equation 23*, which then becomes:

$$\bar{c}_A(r) = c_1(r_F)\,\psi_1(r) + X_2[c_1(r_F)\,\psi_1(r)]^2 + X_3[c_1(r)\,\psi_1(r)]^3 + \ldots \qquad [24]$$

Non-linear least-squares analysis of the dependence of $\bar{c}_A(r)$ upon $\psi_1(r)$ for a given sedimentation equilibrium distribution in terms of this expression with $\psi_1(r)$ as the independent variable thus yields the association constants (X_2, X_3, ...) and $c_1(r_F)$ as the evaluated curve-fitting parameters. In order to accommodate data
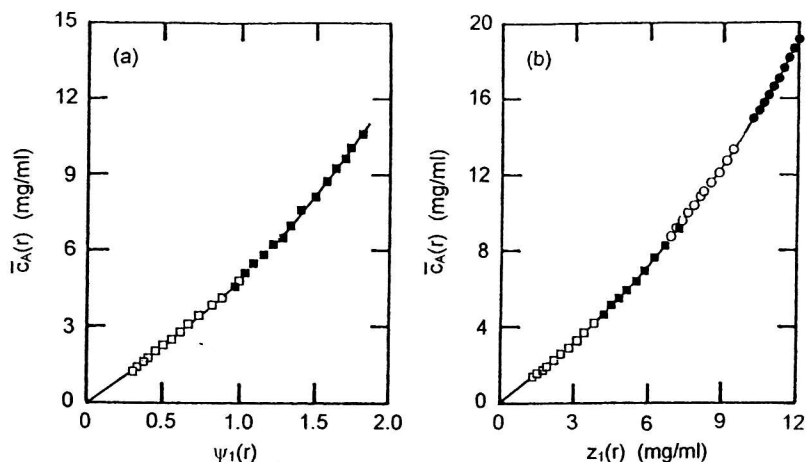
127

Figure 11 Characterization of lysozyme self-association (pH 8.0, I 0.15, 15 °C) by direct analysis of sedimentation equilibrium distributions. (a) Dependence of total solute concentration upon $\psi_1(r)$ evaluated from two sedimentation equilibrium distributions on lysozyme by choosing r_F in each experiment to achieve a common value of $c_A(r_F)$: also shown is the best-fit description obtained by non-linear regression analysis in terms of *Equation 24*. (b) Dependence of total lysozyme concentration upon the thermodynamic activity of monomer obtained by global analysis of four separate sedimentation equilibrium distributions, including those analysed in (a), on the basis of a common reference radial position (r_F) of 7.05 cm. Data in (a) and (b) are taken from refs 13 and 39 respectively.

from several sedimentation equilibrium distributions into a global analysis, the initial approach (13) was to tie the $\psi_1(r)$ scales for separate data sets by selecting individual reference radial positions (r_F) corresponding to the same total solute concentration $\bar{c}_A(r_F)$—the approach illustrated in *Figure 11a*. An alternative procedure (39) simply entails concomitant analysis of solute distributions from all experiments to obtain a global best-fit value of each equilibrium constant as well as the corresponding $c_1(r_F)$ estimate for each run. Despite differences in the values of $c_1(r_F)$ from the individual experiments, the results are amenable to collective display as a dependence of $\bar{c}_A(r)$ upon the magnitude of $c_1(r) = \psi_1(r)c_1(r_F)$. This feature of the global psi analysis is illustrated in *Figure 11b*, where expression of the abscissa in terms of the thermodynamic activity of monomer (rather than its concentration) emphasizes the ability of the direct approach to make rigorous allowance for the effects of thermodynamic non-ideality on the statistical-mechanical basis of excluded volume (13, 39).

The software packages that are provided with Beckman ultracentrifuges for the analysis of solute self-association are based on the Yphantis method of direct analysis (59), which is equivalent to the above procedure for ideal systems. However, the allowance for thermodynamic non-ideality that is incorporated therein is based on the Adams and Fujita assumption (40) that thermodynamic activities are given by the expression $z_i(r) = iBM_1\bar{c}_A(r)$, where B is an empirical curve-fitting parameter. This assumption implies that thermodynamic non-ideality does not influence the extent of solute self-association because self-cancellation of its

128

effects has been designed in the ratio of activity coefficients that relate the apparent and true equilibrium constants (60, 61). It is therefore hoped that the programs will soon be upgraded to accommodate more realistic allowance for the effects of thermodynamic non-ideality.

4.1.3 Earlier procedures for characterizing two-state self-association

For an ideal monomer–dimer system the application of *Equation 24* in the form:

$$\bar{c}_A(r)/\,\psi_1(r) = c_1(r_F) + X_2[c_1(r_F)]^2\psi_1(r) \qquad [25]$$

allows $c_1(r_F)$ to be obtained as the ordinate intercept of the dependence of $\bar{c}_A(r)/\psi_1(r)$—a feature illustrated in *Figure 12a* for the dimerization ($2\alpha\beta \longleftrightarrow \alpha_2\beta_2$) of aquomethaemoglobin (pH 6.0, $I = 0.10$). Furthermore, combination of the consequent value of $c_1(r_F)$ with the magnitude of the slope, $X_2[c_1(r_F)]^2$, yields a dimerization constant of (2.0 ± 0.2) litre/g under these conditions (56).

Prior to the development of direct analytical procedures for the determination of X_2, weight-average molecular weights were used to evaluate the concentration of monomeric acceptor associated with the total acceptor concentration to which $\bar{M}_A$ referred. From the definition of the weight-average molecular weight for a monomer–dimer system, namely:

$$\bar{M}_A = [c_1M_1 + (\bar{c}_A - c_1)M_2]/\bar{c}_A \qquad [26a]$$

the concentration of monomeric acceptor may be obtained as:

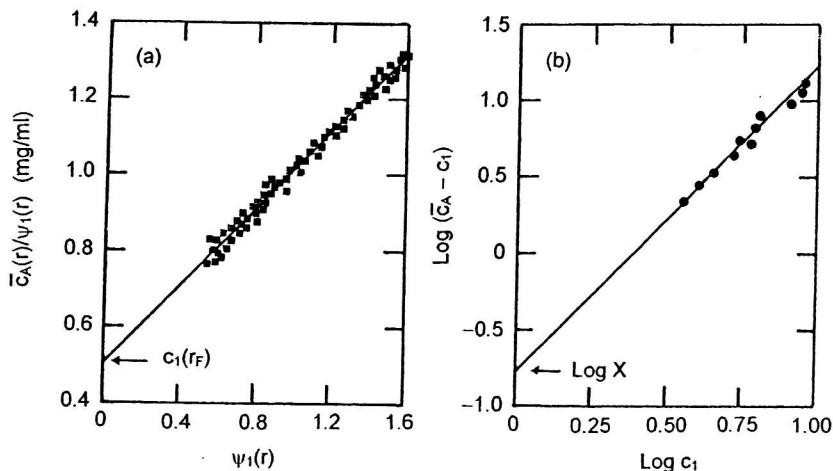$$c_1 = \bar{c}_A(M_2 - \bar{M}_A)/ (M_2 - M_1) \qquad [26b]$$

Figure 12 Earlier methods of characterizing acceptor dimerization by sedimentation equilibrium. (a) Direct analysis of sedimentation equilibrium distributions for methaemoglobin (pH 6.0, $I = 0.10$) in terms of *Equation 25*. (b) Use of *Equation 27* to characterize the dimerization of α-chymotrypsin (pH 7.8, $I = 0.28$) from $[\bar{c}_A, c_1]$ data obtained by molecular weight analysis (*Equation 26*) of sedimentation equilibrium distributions. Data in (a) and (b) are taken from refs 56 and 50 respectively.

Evaluation of X_2 from a series of $[\bar{c}_A, c_1]$ data thus generated may then be accomplished by plotting the results according to the expression:

$$\log(\bar{c}_A - c_1) = \log X_2 + 2\log c_1 \qquad [27]$$

which is the logarithmic form of the law of mass action for a monomer–dimer equilibrium. The application of this procedure to obtain $\log X_2$ from the ordinate intercept of the dependence of $\log(\bar{c}_A - c_1)$ upon $\log c_1$ is illustrated in *Figure 12b*, which refers to the dimerization of α-chymotrypsin in phosphate buffer, pH 7.8, I 0.28 (50).

4.2 Displacement of an acceptor self-association equilibrium by ligand binding

For purposes of illustration we consider a monomer–dimer acceptor system in which ligand (B) binds to p equivalent and independent sites on monomer with intrinsic binding constant k_{1B}, and to q such sites on dimeric acceptor with intrinsic constant k_{2B}. From considerations of mass conservation it follows that the total weight-concentration of acceptor, $\bar{c}_A$, is given by:

$$\bar{c}_A = \bar{c}_1 + \bar{c}_2 = c_1(1 + k_{1B}C_B)^p + c_2(1 + k_{2B}C_B)^q \qquad [28]$$

where $\bar{c}_1$ and $\bar{c}_2$ are the respective constituent concentrations of monomeric and dimeric forms of acceptor. Provided that B is sufficiently small to justify the approximations that $M_{1B_i} \approx M_1$ and $M_{2B_i} \approx M_2$ for all values of i ($0 \leq i \leq p$ and $0 \leq i \leq q$ for monomeric and dimeric states respectively), the effect of ligand binding on the monomer–dimer equilibrium position can be monitored by measuring the constitutive dimerization constant, $\bar{X}_2$, defined (51) as:

$$\bar{X}_2 = \bar{c}_2/\bar{c}_1{}^2 = \bar{X}_2(1 + k_{2B}C_B)^q/(1 + k_{1B}C_B)^{2p} \qquad [29]$$

where X_2 is the dimerization constant measured in the absence of B. Except for the situation in which ligand binding occurs independently of acceptor self-association ($k_{1B} = k_{2B}$, $q = 2p$), the binding of a small ligand is manifested as a dependence of $\bar{X}_2$ upon free ligand concentration C_B. For data obtained by sedimentation equilibrium of a dimerizing acceptor solution in dialysis equilibrium with a free concentration C_B of ligand, the parameters to emerge from application of *Equation 25* are $\bar{c}_1(r_F)$ and $\bar{X}_2$. Alternatively, analysis of the distributions by means of *Equations 26* and *27* lead to values of $\bar{c}_1$ and $\log \bar{X}_2$.

Preferential binding of ligand to one oligomeric state of acceptor leads to several forms of the dependence of $\bar{X}_2$ upon C_B, which therefore provides a powerful means of probing the relative affinities of monomeric and dimeric acceptor states for ligand. This aspect of sedimentation equilibrium studies is illustrated by considering the effects of ligand binding on several self-associating acceptor systems.

4.3 Illustrative studies of preferential ligand binding by sedimentation equilibrium

The binding of *N*-acetylglucosamine to lysozyme affords an example of preferential binding despite the fact that monomeric and polymeric states of the
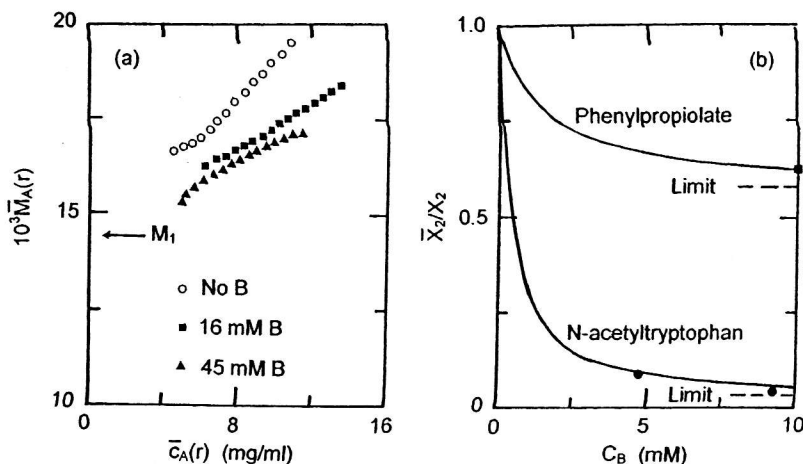
Figure 13 Use of sedimentation equilibrium to monitor perturbation of acceptor self-association as the result of preferential binding of a small ligand to one acceptor state. (a) Effect of *N*-acetylglucosamine on the weight-average molecular weight of lysozyme, pH 8.0, $I = 0.15$ (52). (b) Dependence of the constitutive dimerization constant for α-chymotrypsin upon the concentration of two competitive inhibitors. Lines denote the theoretical dependencies predicted by *Equation 29* for phenylpropiolate ($k_{2B} = 0.76k_{1B}$) and *N*-acetyltryptophan ($k_{2B} = 0.19k_{1B}$). Experimental data are taken from refs 50 and 55.

enzyme exhibit equal affinities for ligand ($k_{1B} = k_{2B}$). Because the active site is involved in the head-to-tail association of lysozyme, there is only one binding site for *N*-acetyltryptophan on each acceptor state (52, 53). In keeping with the qualitative predictions of *Equation 29* for a system with $k_{1B} = k_{2B}$ and $q < 2p$, the extent of self-association decreases with increasing ligand concentration—an effect evident from the dependence of weight-average molecular weight of lysozyme upon *N*-acetylglucosamine concentration (*Figure 13a*). However, departure of the system from a two-state self-association (*Figure 11*) precludes its use to illustrate quantitatively the prediction (*Equation 29*) that $\bar{X}_2 \rightarrow 0$ as $C_B \rightarrow \infty$.

Although sites are conserved ($q = 2$, $p = 1$) in the dimerization of α-chymotrypsin, competitive inhibitors such as phenylpropiolate (50) and *N*-acetyltryptophan (55) bind preferentially to monomeric enzyme because $k_{1B} > k_{2B}$. In keeping with the predictions of *Equation 29*, $\bar{X}_2$ again decreases with increasing ligand concentration (*Figure 13b*). For these systems, however, the predicted limiting magnitude of $\bar{X}_2$ is given by:

$$\lim_{C_B \rightarrow \infty} \bar{X}_2 = X_2(k_{2B}/k_{1B})^q \qquad [30]$$

whereupon a limiting value of zero for $\bar{X}_2$ would implicate exclusive binding of ligand to monomer ($k_{2B} = 0$). For the interactions of phenylpropiolate and *N*-acetyltryptophan with α-chymotrypsin these limits are finite because $k_{2B} = 0.76k_{1B}$ and $0.19k_{1B}$ for the respective ligands (50, 55).

The same limiting expression applies to the preferential interaction of ligands with dimeric acceptor under conditions of site conservation ($q = 2p$, $k_{2B} > k_{1B}$),
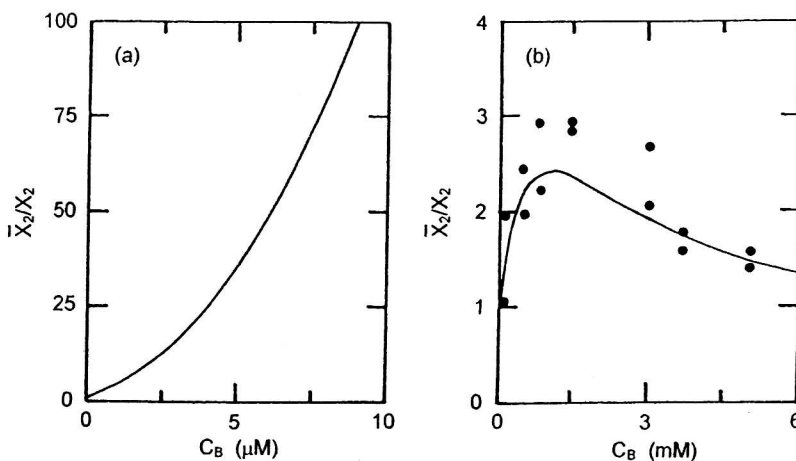
Figure 14 Further examples of the perturbation of acceptor dimerization as the result of preferential ligand binding. (a) Predicted effect of Zn^{2+} concentration on the constitutive binding constant for bacterial α-amylase—a system involving exclusive binding of the metal ion to a single site on dimer (54). (b) Dependence of the constitutive dimerization constant for methaemoglobin upon NADH concentration (56)—a system with $k_{2B} > k_{1B}$ but $q < 2p$ ($p = q = 1$).

but $\bar{X}_2$ now exhibits a positive dependence upon C_B. A ligand-mediated increase in $\bar{X}_2$ without limit is predicted for the binding of Zn^{2+} to bacterial α-amylase (*Figure 14a*), a system for which binding is restricted to a single site on dimer; i.e. a system for which $q = 1$, p and/or $k_{1B} = 0$ (54).

Finally, the interaction of methaemoglobin with NADH (56) and other organophosphate analogues of 2,3-bisphosphoglycerate (51) illustrates the possible existence of a critical point in the dependence of $\bar{X}_2$ upon C_B (*Figure 14b*). Preferential binding is an ambiguous term for this system inasmuch as dimer (the $\alpha_2\beta_2$ species) is the preferred acceptor on the basis of affinity ($k_{2B} > k_{1B}$), whereas monomer ($\alpha\beta$) is the preferred form from the viewpoint of site numbers—one site per base-mole of acceptor compared with one site per two base-moles for dimeric acceptor ($p = 1$, $q = 1$). At low ligand concentrations the magnitude of $\bar{X}_2$ increases with C_B because the binding of a single molecule of organophosphate to the β-cleft of dimer is the dominant phenomenon; but at higher concentrations the denominator of *Equation 29* dominates the magnitude of $\bar{X}_2$, which then decreases with increasing C_B. Non-linear regression analysis of the results in *Figure 14b* according to *Equation 29* with $p = 1$ and $q = 1$ signifies values of (700 ± 100) and (6000 ± 1000) M^{-1} for k_{1B} and k_{2B} respectively (56). A point of interest is that this interplay of equilibria is more amenable to quantitative characterization by sedimentation equilibrium than by classical binding studies.

4 Concluding remarks

Sedimentation equilibrium has much to offer for the quantitative characterization of acceptor–ligand interactions for systems in which both reactants are

macromolecular. Its use for the study of the interaction between a small ligand and a macromolecular acceptor is limited unless the ligand has a unique spectral characteristic that allows analysis of the equilibrium distribution for that constituent. On the other hand, sedimentation equilibrium has played a vital role in characterizing the interplay of equilibria responsible for ligand perturbation of acceptor self-association as the result of preferential binding of a small ligand to one oligomeric state. In this review attention has been confined to the study of macromolecular interactions on the basis of thermodynamic ideality on the grounds that this assumption is a reasonable approximation for the relatively dilute solutions that are use in most *in vitro* studies. However, rigorous allowance for the effects of thermodynamic non-ideality on the statistical-mechanical basis of excluded volume has been incorporated into the analysis of sedimentation equilibrium distributions reflecting either solute self-association (13, 29, 39) or interaction between dissimilar macromolecular reactants (29, 39).

References

1. Casassa, E. F. and Eisenberg, H. (1964). *Adv. Protein Chem.*, **19**, 287.
2. Nichol, L. W., Owen, E. A., and Winzor, D. J. (1982). *J. Phys. Chem.*, **86**, 5015.
3. Van Holde, K. E. and Baldwin, R. L. (1958). *J. Phys. Chem.*, **62**, 734.
4. Correia, J. J. and Yphantis, D. A. (1992). In *Analytical ultracentrifugation in biochemistry and polymer science* (ed. S. E. Harding, A. J. Rowe, and J. C. Horton), p. 231. Royal Society of Chemistry, Cambridge.
5. Hexner, P. E., Radford, L. E., and Beams, J. W. (1961). *Proc. Natl. Acad. Sci. USA*, **74**, 2515.
6. Howlett, G. J. and Nichol, L. W. (1972). *J. Phys. Chem.*, **76**, 2740.
7. Svedberg, T. and Pedersen, K. O. (1940). *The ultracentrifuge.* Clarendon Press, Oxford.
8. Goldberg, R. J. (1953). *J. Phys. Chem.*, **57**, 194.
9. Williams, J. W., Van Holde, K. E., Baldwin, R. L., and Fujita, H. (1958). *Chem. Rev.*, **58**, 715.
10. Haschemeyer, R. H. and Bowers, W. F. (1970). *Biochemistry*, **9**, 435.
11. Milthorpe, B. K., Jeffrey, P. D., and Nichol, L. W. (1975). *Biophys. Chem.*, **3**, 169.
12. Wills, P. R. and Winzor, D. J. (1992). In *Analytical ultracentrifugation in biochemistry and polymer science* (ed. S. E. Harding, A. J. Rowe, and J. C. Horton), p. 311. Royal Society of Chemistry, Cambridge.
13. Wills, P. R., Jacobsen, M. P., and Winzor, D. J. (1996). *Biopolymers*, **38**, 119.
14. Jacobsen, M. P., Wills, P. R., and Winzor, D. J. (1996). *Biochemistry*, **35**, 13173.
15. Wills, P. R., Jacobsen, M. P., and Winzor, D. J. (1997). *Prog. Colloid Polym. Sci.*, **107**, 1.
16. Voelker, P. (1995). *Prog. Colloid Polym. Sci.*, **99**, 162.
17. Yphantis, D. A. (1964). *Biochemistry*, **3**, 297.
18. Creeth, J. M. and Harding, S. E. (1982). *J. Biochem. Biophys. Methods*, **7**, 25.
19. Cölfen, H. and Harding, S. E. (1997). *Eur. J. Biophys.*, **25**, 333: see also Harding, S. E., Horton, J. C., and Morgan, P. J. (1992). In *Analytical ultracentrifugation in biochemistry and polymer science* (ed. S. E. Harding, A. J. Rowe, and J. C. Horton), p. 275. Royal Society of Chemistry, Cambridge.
20. Hall, D. R., Harding, S. E., and Winzor, D. J. (1999). *Prog. Coll. Polym. Sci.*, **113**, 62.
21. Richards, E. G., Teller, D. C., and Schachman, H. K. (1968). *Biochemistry*, **7**, 1054.
22. Winzor, D. J., Jacobsen, M. P., and Winzor, D. J. (1998). *Biochemistry*, **37**, 2226.

23. Nichol, L. W. and Ogston, A. G. (1965). *J. Phys. Chem.*, **69**, 4365.

24. Adams, E. T., Jr. (1969). *Ann. N. Y. Acad. Sci.*, **164**, 226.

25. Hancock, D. K. and Williams, J. W. (1969). *Biochemistry*, **8**, 2598.

26. Teller, D. C., Horbett, T. A., Richards, E. G., and Schachman, H. K. (1969). *Ann. N. Y. Acad. Sci.*, **164**, 66.

27. Roark, D. E. and Yphantis, D. A. (1969). *Ann. N. Y. Acad. Sci.*, **164**, 245.

28. Van Holde, K. E., Rossetti, G. P., and Dyson, R. D. (1969). *Ann. N. Y. Acad. Sci.*, **164**, 279.

29. Wills, P. R., Jacobsen, M. P., and Winzor, D. J. (1998). *Biochem. Soc. Trans.*, **26**, 741.

30. Laue, T. M., Senear, D. F., Eaton, S., and Ross, A. J. B. (1993). *Biochemistry*, **32**, 2469.

31. Kim, T., Tsukiyama, T., Lewis, M. S., and Wu, C. (1994). *Protein Sci.*, **3**, 1040.

32. Lewis, M. S., Shrager, R. I., and Kim, S. J. (1994). In *Modern analytical ultracentrifugation: acquisition and interpretation of data for biological and synthetic polymer systems* (ed. T. M. Schuster and T. M. Laue), p. 94. Birkhäuser, Boston, MA.

33. Bailey, M. F., Davidson, B. E., Minton, A. P., Sawyer, W. H., and Howlett, G. J. (1996). *J. Mol. Biol.*, **263**, 671.

34. Wilson, E. K., Scrutton, N. S., Cölfen, H., Harding, S. E., Jacobsen, M. P., and Winzor, D. J. (1997). *Eur. J. Biochem.*, **243**, 393.

35. Nichol, L. W., Jeffrey, P. D., and Milthorpe, B. K. (1976). *Biophys. Chem.*, **4**, 259.

36. Jeffrey, P. D., Nichol, L. W., and Teasdale, R. D. (1979). *Biophys. Chem.*, **10**, 379.

37. Klotz, I. M. (1946). *Arch. Biochem.*, **9**, 109.

38. Behlke, J., Ristau, O., and Schonfeld, H. J. (1997). *Biochemistry*, **36**, 5149.

39. Wills, P. R., Jacobsen, M. P., and Winzor, D. J. (1999). *Progr. Colloid Polym. Sci.*, **113**, 69.

40. Adams, E. T., Jr. and Fujita, H. (1963). In *Analytical ultracentrifugation in theory and experiment* (ed. J. W. Williams), p. 119. Academic Press, New York.

41. Sophianopoulos, A. J. and Van Holde, K. E. (1964). *J. Biol. Chem.*, **239**, 2516.

42. Sarfare, P. S., Kegeles, G., and Kwon-Rhee, S. J. (1966). *Biochemistry*, **5**, 1389.

43. Adams, E. T., Jr. and Filmer, D. L. (1966). *Biochemistry*, **5**, 2971.

44. Adams, E. T., Jr. and Lewis, M. S. (1968). *Biochemistry*, **7**, 1044.

45. Hoagland, V. D. and Teller, D. C. (1969). *Biochemistry*, **8**, 594.

46. Aune, K. C. and Timasheff, S. N. (1971). *Biochemistry*, **10**, 1609.

47. Howlett, G. J., Jeffrey, P. D., and Nichol, L. W. (1972). *J. Phys. Chem.*, **76**, 777.

48. Morris, M. and Ralston, G. B. (1985). *Biophys. Chem.*, **23**, 49.

49. Nichol, L. W., Jackson, W. J. H., and Winzor, D. J. (1967). *Biochemistry*, **6**, 2449.

50. Nichol, L. W., Jackson, W. J. H., and Winzor, D. J. (1972). *Biochemistry*, **11**, 585.

51. Baghurst, P. A. and Nichol, L. W. (1975). *Biochim. Biophys. Acta*, **412**, 168.

52. Sophianopoulos, A. J. (1969). *J. Biol. Chem.*, **244**, 3188.

53. Howlett, G. J. and Nichol, L. W. (1972). *J. Biol. Chem.*, **247**, 5681.

54. Tellam, R., Winzor, D. J., and Nichol, L. W. (1978). *Biochem. J.*, **173**, 185.

55. Tellam, R., de Jersey, J., and Winzor, D. J. (1979). *Biochemistry*, **18**, 5316.

56. Jacobsen, M. P. and Winzor, D. J. (1995). *Biochim. Biophys. Acta*, **1246**, 17.

57. Steiner, R. F. (1952). *Arch. Biochem. Biophys.*, **39**, 333.

58. Adams, E. T., Jr. and Williams, J. W. (1964). *J. Am. Chem. Soc.*, **86**, 3454.

59. Johnson, M. L., Correia, J. J., Yphantis, D. A., and Halvorson, H. R. (1981). *Biophys. J.*, **36**, 575.

60. Ogston, A. G. and Winzor, D. J. (1975). *J. Phys. Chem.*, **79**, 2496.

61. Jacobsen, M. P. and Winzor, D. J. (1992). *Biophys. Chem.*, **45**, 119.

62. Creeth, J. M. and Pain, R. H. (1967). *Prog. Biophys. Mol. Biol.*, **17**, 217.

63. Teller, D. C. (1973). In *Methods in Enzymology*, Vol. 27, p. 346

64. McRorie, D. K. and Voelker, P. J. (1993). *Self-associating systems in the analytical ultracentrifuge*. Beckman Instruments, Fullerton, California.

65. ftp://alpha.bbri.org/rasmb/spin/mac/nonlin-uconn_uaf/

66. Colfen, H. and Winzor, D. J. (1997). *Prog. Colloid Polym. Sci.*, **107**, 36.

67. Harding, S. E., Horton, J. C., Jones, S., Thornton, J. M., and Winzor, D. J. (1999). *Biophys. J.*, **76**, 2432.